

Higgs-Portal Stueckelberg Dark Matter

Antonio De Felice^{1,*}, Takehiro Ogura^{2,†},
 Shinji Tsujikawa^{3,§}, Kimiko Yamashita^{2,¶}

¹*Center for Gravitational Physics and Quantum Information, Yukawa Institute for Theoretical Physics, Kyoto University, 606-8502, Kyoto, Japan*

²*Department of Physics, Ibaraki University, Mito 310-8512, Japan*

³*Department of Physics, Waseda University, 3-4-1 Okubo, Shinjuku, Tokyo 169-8555, Japan*

^{*}antonio.defelice@yukawa.kyoto-u.ac.jp, [†]25nm014a@vc.ibaraki.ac.jp,

[§]tsujikawa@waseda.jp, [¶]kimiko.yamashita.nd93@vc.ibaraki.ac.jp

Abstract

We study dark photon dark matter X associated with a dark $U(1)_X$ gauge symmetry. To evade laboratory and cosmological constraints on kinetic mixing with the Standard Model $U(1)_Y$, we assign a Z_2 -odd dark parity to X that forbids such mixing. The leading interactions then arise from gauge-invariant dimension-6 Higgs-portal operators, including both parity-even and parity-odd terms. We assume that the dark matter mass is generated via the Stueckelberg mechanism, which also induces a dimension-4 Higgs-portal operator $(H^\dagger H)X_\mu X^\mu$ and additional dimension-6 operators. We investigate freeze-in production of X from Higgs-pair annihilations after reheating, incorporating both gauge-invariant and Stueckelberg-induced operators. First, we consider the case in which the Wilson coefficients of the gauge-invariant dimension-6 operators, C and \tilde{C} , are of order unity. We find that, in this case, the Stueckelberg contributions remain subdominant in dark matter production. This result follows from the requirement that the effective scale implied by perturbative unitarity must exceed the cutoff scale of the effective field theory. Next, we explore a more general situation in which C and \tilde{C} are smaller than unity. In this second case, Stueckelberg-induced operators can become comparable and lead to distinctive features in the dark-matter parameter space, including interference effects. For both cases, we show that there exists a wide parameter space consistent with the observed dark matter relic density.

1 Introduction

Dark photons, the gauge bosons of an additional $U(1)_X$ symmetry, have been extensively studied as mediators between the dark sector and the Standard Model (SM) [1] (see [2] for a review). In the conventional setup, the dark photon interacts with the SM particles through kinetic mixing with the $U(1)_Y$ field strength. However, current laboratory and cosmological constraints severely restrict the allowed kinetic mixing parameter across a wide mass range [3]. For TeV-scale dark photons, collider constraints lead to a quartic suppression of the small mixing angle in the cross section of $pp \rightarrow X \rightarrow \ell\ell$ at the 13 TeV Large Hadron Collider, yielding values well below the order of fb for a mixing angle of 0.01 [4].

Motivated by these limitations on tiny or relatively small mixing angles, our previous work (by one of the authors, KY) [4] considered a scenario in which kinetic mixing is forbidden by imposing a dark Z_2 parity under which the dark photon is odd and all SM fields are even. In this setup, the leading interactions arise from gauge-invariant dimension-6 Higgs-portal operators, namely $(H^\dagger H)X_{\mu\nu}X^{\mu\nu}$ and $(H^\dagger H)\tilde{X}_{\mu\nu}X^{\mu\nu}$, allowing the dark photon to be stable and serve as a viable dark matter (DM) candidate. In that work, KY studied the thermal freeze-out production mechanism and identified the parameter space consistent with the observed DM relic density and direct-detection bounds. In the limit of vanishing momentum transfer, the parity-odd operator is irrelevant for direct detection, whereas the parity-even operator is strongly constrained. Consequently, the activation of the parity-odd operator is essential to achieve the observed DM relic density.

In this work, we examine the freeze-in production of DM and extend the previous scenario by adopting the Stueckelberg mechanism as the origin of the dark photon mass. The Stueckelberg mass generation preserves the “ $U(1)_X$ gauge symmetry”*. Without introducing a dark scalar to generate the mass (as in the Higgs mechanism), the mass term is instead realized through the Stueckelberg framework, which remains valid only at energies below the scale at which perturbative unitarity is violated. A crucial consequence is that the operator $(H^\dagger H)X_\mu X^\mu$ now appears at dimension 4[†], and two additional dimension-6 operators relevant to the annihilation of Higgs pairs into DM pairs also emerge, on top of the gauge-invariant dimension-6 operators considered previously. We investigate the freeze-in production of Stueckelberg dark photon DM through the Higgs portal, incorporating all the dimension-4 and dimension-6 interactions.

The paper is organized as follows. In Section 2, we review the dimension-6 Higgs-portal

*The vector field remains invariant under the gauge symmetry. Here, the prime is used to indicate the “fake” $U(1)_X$ gauge symmetry [5].

[†]The thermal relic abundance of a weakly interacting massive particle arising from this Stueckelberg-induced dimension-4 operator is discussed in Ref. [6] by Lebedev, Lee, and Mambrini.

dark photon model of Ref. [4] and introduce its Stueckelberg extension. In Section 3, we compute the DM relic density via Higgs-portal freeze-in, taking into account the gauge-invariant parity-even and parity-odd dimension-6 terms, and identify the viable parameter space. We also discuss the additional operators arising from the Stueckelberg mechanism and compute the corresponding DM relic density, focusing on the parameter region in which their contributions become relevant alongside the gauge-invariant dimension-6 operators. A summary is presented in Sec. 4.

2 Higgs-Portal Dark Photon with Stueckelberg Mass

In this section, we first briefly review the Higgs-portal dark photon DM model up to dimension-6 operators, following Ref. [4]. We then introduce the Stueckelberg mechanism for generating the dark photon mass without explicitly introducing a dark scalar.

2.1 Higgs-Portal Interactions at Dimension-6

Here, we briefly review the dark photon DM model discussed in Ref. [4]. We consider a dark photon associated with an additional dark gauge symmetry $U(1)_X$, where the dark photon is odd under a dark parity, whereas all SM fields are neutral under $U(1)_X$ and even under the dark parity. In this setup, kinetic mixing is absent, and the dark photon can serve as a viable DM candidate.

The gauge-invariant interactions between the dark photon and the SM particles up to dimension 6 are described by the Higgs-portal operators:

$$\mathcal{O} = (H^\dagger H) X_{\mu\nu} X^{\mu\nu}, \quad (1)$$

$$\tilde{\mathcal{O}} = (H^\dagger H) \tilde{X}_{\mu\nu} X^{\mu\nu}, \quad (2)$$

where H is the SM Higgs doublet, $X_{\mu\nu} = \partial_\mu X_\nu - \partial_\nu X_\mu$ is the field strength of the dark photon DM X_μ , and $\tilde{X}_{\mu\nu} = (1/2)\epsilon_{\mu\nu\rho\sigma} X^{\rho\sigma}$ is its dual, with $\epsilon_{0123} = 1$. The operator $\tilde{\mathcal{O}}$ is odd under parity and time-reversal transformations due to the presence of the Levi-Civita tensor $\epsilon_{\mu\nu\rho\sigma}$.

The effective Lagrangian describing a dark photon with mass m_X and its interactions with the SM particles up to dimension-6 is given by

$$\mathcal{L}_{\text{VDM}} = \frac{m_X^2}{2} X_\mu X^\mu + \frac{C}{\Lambda^2} \mathcal{O} + \frac{\tilde{C}}{\Lambda^2} \tilde{\mathcal{O}}, \quad (3)$$

where C and \tilde{C} are the Wilson coefficients associated with the operators in Eqs. (1) and (2), Λ denotes the characteristic energy scale of new physics.

We employ the Stueckelberg mechanism to generate the dark photon mass, as described in the following Section 2.2.

2.2 Higgs-Portal Stueckelberg Dark Photon DM up to Dimension-6

To generate the mass of the dark photon without introducing an explicit dark scalar, we employ the Stueckelberg mechanism (see [7] for review). In this setup, the dark photon acquires a mass while preserving the “ $U(1)_X$ gauge symmetry”, and the dark parity $X^\mu \rightarrow -X^\mu$ ensures the stability of the dark photon as a DM candidate.

In the Stueckelberg mechanism, we define a “fake” $U(1)_X$ gauge field [5]:

$$A^\mu \equiv X^\mu + \frac{\partial^\mu \pi}{m_X}, \quad (4)$$

where π is a Stueckelberg scalar field. Both fields transform under this “ $U(1)$ gauge transformation” as

$$A^\mu \rightarrow A^\mu + \partial^\mu \chi, \quad (5)$$

$$\pi \rightarrow \pi + m_X \chi, \quad (6)$$

where $\chi(x)$ is the gauge parameter. Under these transformations (5) and (6), X^μ in Eq. (4) is invariant.

Therefore, in a Lagrangian, a Proca mass contribution for X^μ is not incompatible with this $U(1)$ gauge symmetry. In fact, we can write

$$\mathcal{L} \supset \frac{1}{2} m_X^2 X^\mu X_\mu = \frac{1}{2} (\partial_\mu \pi - m_X A_\mu) (\partial^\mu \pi - m_X A^\mu). \quad (7)$$

This construction allows terms in the Lagrangian as the following one

$$\mathcal{L} \supset \frac{\bar{\lambda}_{HX}}{\Lambda^2} (\partial_\mu \pi - m_X A_\mu) (\partial^\mu \pi - m_X A^\mu) H^\dagger H. \quad (8)$$

This mass term effectively gives a kinetic term for the field π . Note that no kinetic term for π comes instead from the term $-(1/4) F_{\mu\nu}^X F^{X\mu\nu}$, since $F_{\mu\nu}^X = \partial_\mu X_\nu - \partial_\nu X_\mu = \partial_\mu A_\nu - \partial_\nu A_\mu$. We can make use of the $U(1)$ gauge symmetry to set a gauge fixing. The Lorenz fixing is a possibility, but we are going to adopt the gauge for which $\pi = 0$. In this case, the above dimension-6 operator can be rewritten as a dimension-4 operator as

$$\mathcal{L}_X = \lambda_{HX} (H^\dagger H) X_\mu X^\mu, \quad (9)$$

which is consistent with the transformations in (5) and (6) and the dark parity, and we have set

$$\lambda_{HX} = \bar{\lambda}_{HX} (m_X^2 / \Lambda^2). \quad (10)$$

Along the same lines, we can introduce a dimension-8 operator as follows:

$$\mathcal{L} \supset 2 \frac{\bar{C}_X}{\Lambda^4} (\partial_\mu \pi - m_X A_\mu) (\partial^\mu \pi - m_X A^\mu) |D_\nu H|^2. \quad (11)$$

We will consider such an operator in more detail later on. Once more, after fixing the $\pi = 0$ gauge, this operator can be rewritten as a dimension-6 operator, namely $(C_X / \Lambda^2) |D_\mu H|^2 X_\nu X^\nu$ with $C_X = 2\bar{C}_X m_X^2 / \Lambda^2$.

Note that once the SM Higgs acquires a vacuum expectation value $v = 246$ GeV, the dark photon mass is shifted as

$$m_X^2 \rightarrow m_X^2 + \lambda_{HX} v^2. \quad (12)$$

For freeze-in DM production near the reheating temperature, we assume that the electroweak symmetry is unbroken, so that the DM mass originates solely from the Stueckelberg mass term during this epoch. To avoid a negative mass squared in the late Universe, we require

$$\lambda_{HX} \geq 0 \quad \text{or} \quad (\lambda_{HX} < 0 \text{ and } m_X^2 > |\lambda_{HX}| v^2). \quad (13)$$

A notable feature of the dimension-4 Higgs-portal Stueckelberg operator is that the scattering amplitude for longitudinal modes grows with the center-of-mass energy as powers of \sqrt{s}/m_X . This growth leads to a violation of perturbative unitarity at high energies, which results in the condition [5]:

$$s_{\max} \simeq \frac{m_X^2}{\lambda_{HX}}. \quad (14)$$

Correspondingly, the cutoff of this Effective Field Theory (EFT) is approximately

$$\Lambda_X \simeq \frac{m_X}{\sqrt{\lambda_{HX}}}, \quad (15)$$

which must be taken into account when analyzing Higgs-portal Stueckelberg DM production. This behavior contrasts with the dimension-4 Higgs-portal scalar DM operator $(H^\dagger H)\phi^2$ involving a scalar DM field ϕ , for which the scattering amplitude does not exhibit any growth with s .

We also consider the following dimension-6 Higgs-portal Stueckelberg operators, which contribute to the 2-to-2 scattering of a Higgs pair into a DM pair in the electroweak-symmetric phase, in addition to Eqs. (1) and (2):

$$\mathcal{O}_X = |D_\mu H|^2 X_\nu X^\nu, \quad (16)$$

$$\tilde{\mathcal{O}}_X = i(H^\dagger \overleftrightarrow{D^\mu} H) \tilde{X}_{\mu\nu} X^\nu. \quad (17)$$

All of these operators are suppressed by Λ^2 . Note that $(\partial^\mu \partial^\nu |H|^2) X_\mu X_\nu$, $i(H^\dagger \overleftrightarrow{D^\mu} H) X_{\mu\nu} X^\nu$, and $((H^\dagger D_\mu H) X^\nu \partial^\mu X_\nu + \text{h.c.})$ are redundant when using the field equations of motion. We do not include $\tilde{\mathcal{O}}_X$ in Eq. (17) in our analysis, as we have confirmed that it contributes to the squared amplitude in the freeze-in process with a suppression of $\mathcal{O}(m_X^2/s) \simeq \mathcal{O}(m_X^2/T_{\text{reh}}^2) \ll 1$ compared to the contribution from \mathcal{O}_X . Here, T_{reh} denotes the reheating temperature, and we assume $T_{\text{reh}} > m_X$, as will be discussed later.

The full effective Lagrangian considered in this work is

$$\mathcal{L}_{\text{VDM}} = \frac{m_X^2}{2} X_\mu X^\mu + \frac{C}{\Lambda^2} \mathcal{O} + \frac{\tilde{C}}{\Lambda^2} \tilde{\mathcal{O}} + \lambda_{HX} (H^\dagger H) X_\mu X^\mu + \frac{C_X}{\Lambda^2} \mathcal{O}_X. \quad (18)$$

For the dimension-6 operator in (16), we determine the effective cutoff scale by requiring that the squared scattering amplitude for the process of Higgs pair to DM pair production be of order unity. This leads to

$$\Lambda_X^{\text{dim-6}} \simeq \frac{2^{1/4} (\Lambda m_X)^{1/2}}{C_X^{1/4}}. \quad (19)$$

For a fully ultraviolet (UV) completion of the Higgs-portal Stueckelberg DM scenario at high energies, one would need to introduce a dark Higgs boson that generates the dark photon mass through the Higgs mechanism. The presence of the dark Higgs restores perturbative unitarity in longitudinal vector boson scattering at high energies [5]. Because of this, the following relation between the cutoff scales should be satisfied [8]:

$$\Lambda_X, \Lambda_X^{\text{dim-6}} > \Lambda. \quad (20)$$

From Eq. (20) together with Eqs. (15) and (19), respectively, we obtain the following conditions:

$$|\lambda_{HX}| < \frac{m_X^2}{\Lambda^2}, \quad \text{or} \quad |\bar{\lambda}_{HX}| < 1, \quad (21)$$

$$|C_X| < 2 \frac{m_X^2}{\Lambda^2}, \quad \text{or} \quad |\bar{C}_X| < 1. \quad (22)$$

This implies that the coefficients are smaller than order unity, as required for the validity of the EFT, i.e. $m_X < \Lambda$. Note that Eq. (13) is automatically satisfied by the condition (21), since $\Lambda > v$. A detailed study of such a UV completion is left for future work.

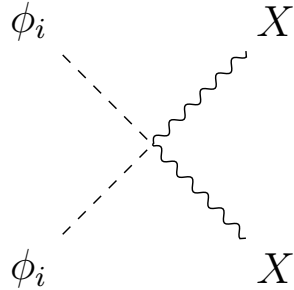


Figure 1: Feynman diagrams for DM production from scalar-pair annihilation within the Higgs doublet. Here, ϕ_i ($i = 1, 2, 3, 4$) denote the four real scalar components of the Higgs doublet, and X represents the real vector DM.

3 DM relic density via Higgs-Portal Freeze-in

In this section, we examine the constraints on the Higgs-portal couplings relevant for the freeze-in production of DM. First, in Sec. 3.1, we briefly review the method used to compute DM freeze-in production, following Ref. [9] by Kim, Lee, and one of the authors (KY). Next, in Sec. 3.2, we present the viable parameter space that reproduces the observed DM relic density using the dimension-6 operators in Eqs. (1)–(3). Then, in Sec. 3.3, we introduce the dimension-4 and dimension-6 operators arising from the Stueckelberg mechanism and show that they can be neglected compared to the gauge-invariant dimension-6 operators. Finally, we consider the case in which the Wilson coefficients of the gauge-invariant dimension-6 operators are suppressed to be smaller than unity, and discuss the DM relic density including the Stueckelberg-induced operators.

3.1 Setup for Freeze-in DM

In this subsection, we briefly review the method for computing the DM freeze-in production following Refs. [9, 10]. In our model, DM is produced through Higgs-portal interactions in the electroweak-symmetric phase, where all four real scalar components of the Higgs doublet contribute equally to the production processes.

The relevant Higgs-portal operators are given by

$$\frac{C}{\Lambda^2}(H^\dagger H) X_{\mu\nu} X^{\mu\nu}, \quad \frac{\tilde{C}}{\Lambda^2}(H^\dagger H) \tilde{X}_{\mu\nu} X^{\mu\nu}, \quad \lambda_{HX}(H^\dagger H) X_\mu X^\mu, \quad \frac{C_X}{\Lambda^2} |D_\mu H|^2 X_\nu X^\nu. \quad (23)$$

The first two terms correspond to the gauge-invariant dimension-6 CP-even and CP-odd Higgs-portal operators, whereas the last two terms are the dimension-4 and dimension-6 operators generated by the Stueckelberg mechanism.

DM is produced via scalar-scalar scattering within the Higgs doublet, namely the process $\phi_i\phi_i \rightarrow XX$ shown in Figure 1 [‡], where ϕ_i ($i = 1, 2, 3, 4$) are the four real scalar components of the Higgs doublet,

$$H = \frac{1}{\sqrt{2}} \begin{pmatrix} \phi_1 + i\phi_2 \\ \phi_3 + i\phi_4 \end{pmatrix}. \quad (24)$$

In the freeze-in mechanism [11–13], the DM must remain out of thermal equilibrium. This condition can be expressed as the reaction rate being smaller than the Hubble expansion rate [14],

$$n_\phi \langle \sigma v \rangle < H, \quad (25)$$

where n_ϕ is the number density of particles in the thermal bath, $\langle \sigma v \rangle$ is the thermally averaged cross section, and H is the Hubble parameter.

For the Higgs-portal Stueckelberg DM, the scattering amplitude for $\phi_i\phi_i \rightarrow XX$ can be roughly estimated by considering the two contributions separately (neglecting interference terms):

$$|\mathcal{M}_{\phi_i\phi_i \rightarrow XX}|^2 \sim \lambda_{HX}^2 \frac{s^2}{m_X^4}, \quad |\mathcal{M}_{\phi_i\phi_i \rightarrow XX}|^2 \sim C_X^2 \frac{s^4}{\Lambda^4 m_X^4}, \quad (26)$$

where s is the Mandelstam variable, which is roughly $s \sim T^2$ for a thermal bath at temperature T . The corresponding thermally averaged cross sections are then estimated as

$$\langle \sigma v \rangle \sim \frac{|\mathcal{M}|^2}{s} \sim \frac{\lambda_{HX}^2 T^2}{m_X^4}, \quad \langle \sigma v \rangle \sim \frac{|\mathcal{M}|^2}{s} \sim \frac{C_X^2 T^6}{\Lambda^4 m_X^4}. \quad (27)$$

Assuming a relativistic thermal bath, $n_\phi \sim T^3$, and comparing with the Hubble expansion rate $H \sim T^2/M_{\text{pl}}$, the freeze-in condition (25) leads to the following upper bounds on the couplings:

$$\lambda_{HX} \lesssim \frac{m_X^2}{(T_{\text{reh}}^3 M_{\text{pl}})^{1/2}}, \quad (28)$$

$$C_X/\Lambda^2 \lesssim \frac{m_X^2}{(T_{\text{reh}}^7 M_{\text{pl}})^{1/2}}, \quad (29)$$

where T_{reh} is the reheating temperature and $M_{\text{pl}} = 2.435 \times 10^{18}$ GeV is the reduced Planck mass. Here we take the reheating temperature as the scale for UV freeze-in in our scenario. In this context, UV freeze-in refers to DM production that occurs predominantly at very high temperatures, close to the reheating scale, where the effective interactions are generated.

[‡]Note that only $\tilde{\mathcal{O}}_X$ in Eq. (17) can contribute to $\phi_1\phi_2 \rightarrow XX$, etc.

Similarly, the gauge-invariant dimension-6 Higgs-portal operators are constrained by [9]

$$C/\Lambda^2, \tilde{C}/\Lambda^2 \lesssim (T_{\text{reh}}^3 M_{\text{pl}})^{-1/2}. \quad (30)$$

For gauge-invariant dimension-6 operators with $C, \tilde{C} = \mathcal{O}(1)$, the minimal cutoff scale required for kinematic decoupling is

$$\Lambda \gtrsim (T_{\text{reh}}^3 M_{\text{pl}})^{1/4}. \quad (31)$$

For example, this implies $\Lambda \gtrsim 10^{15}$ GeV for $T_{\text{reh}} = 10^{14}$ GeV and $\Lambda \gtrsim 10^9$ GeV for $T_{\text{reh}} = 10^6$ GeV. Thus, the cutoff scale typically needs to exceed the reheating temperature by one to three orders of magnitude. In this regime, the unitarity condition is automatically satisfied, which requires $T_{\text{reh}} \lesssim \Lambda$ in the limit where the DM and Higgs masses can be neglected. Eqs. (28) and (29) are automatically satisfied by Eqs. (21) and (22), respectively, together with Eq. (31).

For the dimension-4 and dimension-6 Stueckelberg operators, the UV cutoff scales in Eqs. (15) and (19) are automatically higher than the reheating temperature under the kinematic decoupling conditions:

$$\Lambda_X \gtrsim (T_{\text{reh}}^3 M_{\text{pl}})^{1/4} > T_{\text{reh}}. \quad (32)$$

$$\Lambda_X^{\text{dim-6}} \gtrsim 2(T_{\text{reh}}^7 M_{\text{pl}})^{1/8} > T_{\text{reh}}. \quad (33)$$

However, they must also satisfy Eqs. (21) and (22) to ensure that $\Lambda_X > \Lambda$.

We consider a homogeneous and isotropic cosmological background described by the line element $ds^2 = dt^2 - a^2(t) \delta_{ij} dx^i dx^j$, where $a(t)$ is the scale factor that depends on the cosmic time t . The number density of DM obeys the Boltzmann equation,

$$\dot{n}_X + 3Hn_X = R(T), \quad (34)$$

where a dot denotes the derivative with respect to t , $R(T)$ is the total production rate per unit volume and per unit time, which depends on the background temperature T , and $H \equiv \dot{a}/a$ is the Hubble expansion rate. The DM production occurs during radiation dominance, in which H can be expressed as

$$H = \sqrt{\frac{\rho_R}{3M_{\text{pl}}^2}} = \sqrt{\frac{g_*}{90} \frac{\pi T^2}{M_{\text{pl}}}}, \quad (35)$$

where $\rho_R = \pi^2 g_* T^4 / 30$ is the radiation energy density, and g_* is the number of effective relativistic degrees of freedom (DOFs). Introducing the DM yield $Y_X \equiv n_X/T^3$ and using the property $T \propto a^{-1}$, we obtain

$$\frac{dY_X}{dT} = -\frac{R(T)}{H(T) T^4}. \quad (36)$$

For a general scattering process $AB \rightarrow CD$, the production rate is given by

$$R(T) = g_\phi \int f_A f_B \frac{E_A E_B dE_A dE_B \cos \theta_{AB}}{1024\pi^6} \int |\mathcal{M}_{AB \rightarrow CD}|^2 d\Omega_{AC}, \quad (37)$$

where

$$f_{A,B} = \frac{1}{e^{E_{A,B}/T} - 1} \quad (38)$$

are the Bose–Einstein distributions for the Higgs bosons with the corresponding energies E_A and E_B , respectively. Here, $g_\phi = 4$ is the number of Higgs DOFs, θ_{AB} is the angle between the incoming Higgs bosons A and B in the laboratory frame, $d\Omega_{AC}$ is the solid angle of one of the outgoing particles in the center-of-mass (COM) frame, and $|\mathcal{M}_{AB \rightarrow CD}|^2$ denotes the squared matrix element of the process $AB \rightarrow CD$.

In Eq. (37), we neglect the overall 2-body phase-space factor $\sqrt{1 - 4m_X^2/s}$. This is justified because, as we show in the next sections, the DM yield is dominantly produced around the reheating temperature for the parameter space of interest and when $m_X \ll T_{\text{reh}}$, the overall 2-body phase-space factor can be approximated as unity. If the DM mass is larger than the temperature, $E_A, E_B > m_X > T$, the DM production is exponentially suppressed due to the Boltzmann factors $f_{A,B} \simeq \exp(-E_{A,B}/T)$. We assume that the initial-state Higgs bosons are massless, corresponding to the electroweak-symmetric phase.

The Mandelstam variables, s and t , are related to the angle between the initial states in the laboratory frame, θ_{AB} , and the scattering angle θ_{AC} in the COM frame, as follows:

$$s = 2E_A E_B (1 - \cos \theta_{AB}), \quad (39)$$

$$t = \frac{s}{2} \left(\sqrt{1 - \frac{4m_X^2}{s}} \cos \theta_{AC} - 1 \right) + m_X^2. \quad (40)$$

We can take $d\Omega_{AC} = 2\pi d\cos \theta_{AC}$ due to the azimuthal symmetry in the COM frame. Here, we note that s appearing in t is taken in the COM frame, but its value is identical to the one in the laboratory frame. Thus, we use the form of s in the laboratory frame in Eq. (39), which is appropriate for thermal averages.

The relic density is obtained by integrating Eq. (36) from the reheating temperature down to temperatures of order the Higgs mass, below which the production rate becomes Boltzmann suppressed, i.e., $f_{A,B} \simeq \exp(-E_{A,B}/T)$.

3.2 Gauge-Invariant Dimension-6 Operators

First, in terms of the coefficients of the gauge-invariant Higgs-portal dimension-6 operators, we obtain the squared scattering amplitude for $\phi_i \phi_i \rightarrow XX$ ($i = 1, 2, 3, 4$) by implementing

the model in FeynRules [15–17] and using CalcHEP [18]. The result is given by

$$|\mathcal{M}_{\phi_i\phi_i \rightarrow XX}|^2 = \frac{2}{\Lambda^4} \left[C^2(s^2 - 4m_X^2s + 6m_X^4) + \tilde{C}^2s(s - 4m_X^2) \right], \quad (41)$$

where the symmetry factors for identical particles in both the initial state ($\phi_i\phi_i$) and the final state (XX) are included. The polarization states of the final-state DM (XX) are summed over. Both operators give (s -wave)² contributions in Eq. (41). In the high-energy limit, where $s \gg m_X^2$, the squared scattering amplitude in Eq. (41) can be approximated as

$$|\mathcal{M}_{\phi_i\phi_i \rightarrow XX}|^2 \simeq \frac{2s^2}{\Lambda^4} (C^2 + \tilde{C}^2). \quad (42)$$

Compared to Appendix A of Ref. [9], we find the correspondences $c_{2,0} = 2(C^2 + \tilde{C}^2)$ and $M = \Lambda$. Therefore, the production rate can be obtained from Eq. (42) as

$$R(T) = g_\phi \frac{c_{2,0}}{M^4} \frac{\pi^3 T^8}{5400} \quad (43)$$

$$= g_\phi \frac{C^2 + \tilde{C}^2}{\Lambda^4} \frac{\pi^3 T^8}{2700}. \quad (44)$$

From Eqs. (35) and (44), the right-hand side of Eq. (34) can be expressed as a function of T . We are interested in DM production from the end of reheating, characterized by the temperature T_{reh} , down to the temperature $T = m_h$, at which the Higgs fields become non-relativistic. For temperatures $T < m_h$, the production rate $R(T)$ in Eq. (37) rapidly approaches zero due to the Boltzmann suppression of the distribution functions, $f_{A,B}$. Therefore, for $T < m_h \simeq 125$ GeV, the DM yield Y_X becomes frozen at the value $Y_X(m_h)$. Since the integration of the Boltzmann equation is dominated by high temperatures for the dimension-6 operators considered here, we take g_* to be its value at T_{reh} , i.e., $g_* = g_*(T_{\text{reh}})$, which applies to the UV freeze-in regime with $T_{\text{reh}} \gg m_h$. We use $g_*(T_{\text{reh}}) = 106.75$ for the SM. This justifies working in the electroweak symmetric phase.

Integrating Eq. (36) with respect to T , we obtain

$$Y_X(T) = -2 \times \frac{g_\phi}{\sqrt{g_*(T_{\text{reh}})}} \frac{\pi^2 M_{\text{pl}}(C^2 + \tilde{C}^2)}{270\sqrt{10}\Lambda^4} T^3 + C_{\text{int}}, \quad (45)$$

where C_{int} is an integration constant. Note that a factor of 2 is added to the second term of the DM yield to account for the two DM particles produced in the final state. As the temperature T decreases from T_{reh} to m_h , Y_X increases. The constant C_{int} is determined by the initial condition $Y_X(T) = Y_X(T_{\text{reh}})$ at the end of reheating ($T = T_{\text{reh}}$). At the temperature $T = m_h$, the DM yield is then given by [9]

$$Y_X(m_h) = Y_X(T_{\text{reh}}) + \frac{g_\phi}{\sqrt{g_*(T_{\text{reh}})}} \frac{\pi^2 M_{\text{pl}}(C^2 + \tilde{C}^2)}{135\sqrt{10}\Lambda^4} (T_{\text{reh}}^3 - m_h^3). \quad (46)$$

In the limit $T_{\text{reh}} \gg m_h$ and assuming $Y_X(T_{\text{reh}}) = 0$, Eq. (46) can be approximated as

$$Y_X(m_h) \simeq \frac{g_\phi}{\sqrt{g_*(T_{\text{reh}})}} \frac{\pi^2 M_{\text{pl}}(C^2 + \tilde{C}^2)}{135\sqrt{10}\Lambda^4} T_{\text{reh}}^3. \quad (47)$$

The corresponding DM number density at $T = m_h$ is $n_X(m_h) \propto Y_X(m_h)m_h^3$, so that the DM energy density at $T = m_h$ becomes $\rho_X(m_h) = n_X(m_h)m_X \propto m_h^3 m_X Y_X(m_h)$. Since the DM energy density scales as a^{-3} for $T < m_X$, its present-day value, denoted by $\rho_X^{(0)}$, is given by

$$\rho_X^{(0)} \propto m_h^3 m_X Y_X(m_h) \left[\frac{a_0}{a(m_h)} \right]^{-3}, \quad (48)$$

where a_0 and $a(m_h)$ are the scale factors today and at $T = m_h$, respectively. Due to entropy conservation, $g_{*s}T^3a^3 = \text{constant}$, where g_{*s} denotes the effective entropy DOFs, a comparison between $T = m_h$ and present temperature $T_0 \simeq 2.35 \times 10^{-13} \text{ GeV}$ (measured in the observations of cosmic microwave background) yields

$$\left[\frac{a_0}{a(m_h)} \right]^{-3} \simeq \frac{g_{*s}(T_0)}{g_{*s}(T_{\text{reh}})} \frac{T_0^3}{m_h^3}, \quad (49)$$

where $g_{*s}(T_0) \simeq 3.91$ is the present-day effective entropy DOFs. Here we have used the approximation $g_{*s}(m_h) \simeq g_{*s}(T_{\text{reh}}) = 106.75$ for the value of g_{*s} at $T = m_h$.

The present-day DM density parameter is defined as $\Omega_X = \rho_X^{(0)} / (3M_{\text{pl}}^2 H_0^2)$, where H_0 is the present-day Hubble parameter, given by $H_0 = 2.13 \times 10^{-42} h \text{ GeV}$ (with $h \approx 0.7$). By using Eq. (48) with Eqs. (47) and (49), it follows that

$$\Omega_X h^2 = 1.6 \times 10^8 \left(\frac{m_X}{1 \text{ GeV}} \right) \left(\frac{g_{*s}(T_0)}{g_{*s}(T_{\text{reh}})} \right) Y_X(m_h) \quad (50)$$

$$\simeq 2.3 \times 10^6 \left(\frac{m_X}{1 \text{ GeV}} \right) \frac{\pi^2 M_{\text{pl}}(C^2 + \tilde{C}^2)}{135\sqrt{10}\Lambda^4} T_{\text{reh}}^3 \quad (51)$$

$$\simeq 0.12 \left(\frac{m_X}{100 \text{ GeV}} \right) \left(\frac{T_{\text{reh}}}{10^{10} \text{ GeV}} \right)^3 \left(\frac{10^{14} \text{ GeV}}{\Lambda} \right)^4 \times 1.1(C^2 + \tilde{C}^2). \quad (52)$$

In Figure 2, we show the parameter space in the m_X - T_{reh} plane that reproduces the observed DM relic density, $\Omega_X h^2 = 0.12$ [20]. For the Higgs-portal suppression scale, we take $\Lambda = 10^{13,14,15,16} \text{ GeV}$ in the left panel and $\Lambda = 10^{8,10,12} \text{ GeV}$ in the right panel, while keeping $C = \tilde{C} = 1$ fixed throughout. In the grey regions, the condition for thermal scattering ($m_X < T_{\text{reh}}$) is not satisfied, resulting in Boltzmann-suppressed DM production. DM masses below $\sim 1 \text{ keV}$ are disfavored by Lyman- α bounds [19]. A larger cutoff scale Λ or a lower reheating temperature T_{reh} generally favors a heavier DM mass m_X to achieve $\Omega_X h^2 = 0.12$. Moreover, a smaller cutoff scale Λ requires a lower reheating temperature T_{reh} to reproduce

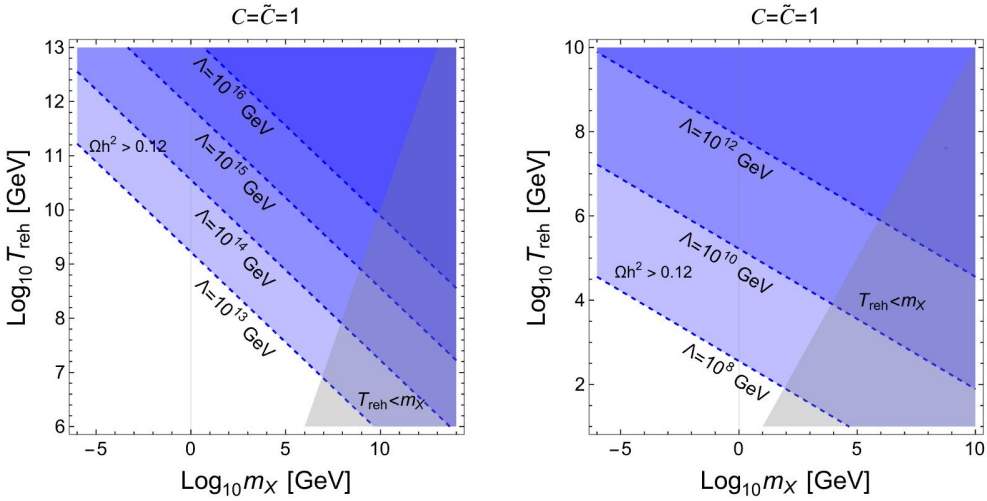


Figure 2: Parameter space in the m_X - T_{reh} plane consistent with the observed DM relic density for $C = \tilde{C} = 1$. In the left and right panels, we take the cutoff scale to be $\Lambda = 10^{13,14,15,16}$ GeV and $\Lambda = 10^{8,10,12}$ GeV, respectively. The grey regions indicate $T_{\text{reh}} < m_X$, where DM production is Boltzmann suppressed. DM masses below 1 keV are excluded from consideration due to Lyman- α constraints on warm DM [19]. The DM relic density is overproduced in the blue region ($\Omega_X h^2 > 0.12$), whereas the observed value is realized along the boundary.

the correct DM abundance. By treating the reheating temperature as a free parameter, we find that a wide range of DM masses and cutoff scales is consistent with the observed DM relic density.

In Figure 3, we present the parameter space in the C - \tilde{C} plane (left) and in the m_X - C ($= \tilde{C}$) plane (right) that reproduces the observed DM relic density. Here, we fix $\Lambda = 10^{16}$ GeV and $T_{\text{reh}} = 10^{12}$ GeV. In the regions outside the allowed boundaries, $\Omega_X h^2$ exceeds 0.12, while the observed value 0.12 is realized along the boundaries. In the left panel, for $m_X = 100$ TeV and $m_X = 10$ TeV, the boundaries corresponding to $\Omega_X h^2 = 0.12$ are given by the circles $C^2 + \tilde{C}^2 \simeq 0.3^2$ and $C^2 + \tilde{C}^2 \simeq 1^2$, respectively. The boundary curves in the right panel of Figure 3 satisfy $|C| \sqrt{m_X/(10^2 \text{ GeV})} \simeq 6.7$, implying that $|C|$ decreases as m_X increases. Figure 4 shows the corresponding parameter space for $\Lambda = 10^{12}$ GeV and $T_{\text{reh}} = 10^8$ GeV. In this case, the correct DM relic density is obtained around $m_X \simeq 1$ GeV for $(C^2 + \tilde{C}^2)^{1/2} \simeq 1$, in agreement with the result in Eq. (52). The lightest allowed DM mass, $m_X \simeq$ keV, constrained by Lyman- α observations, can be realized for lower Λ and T_{reh} .

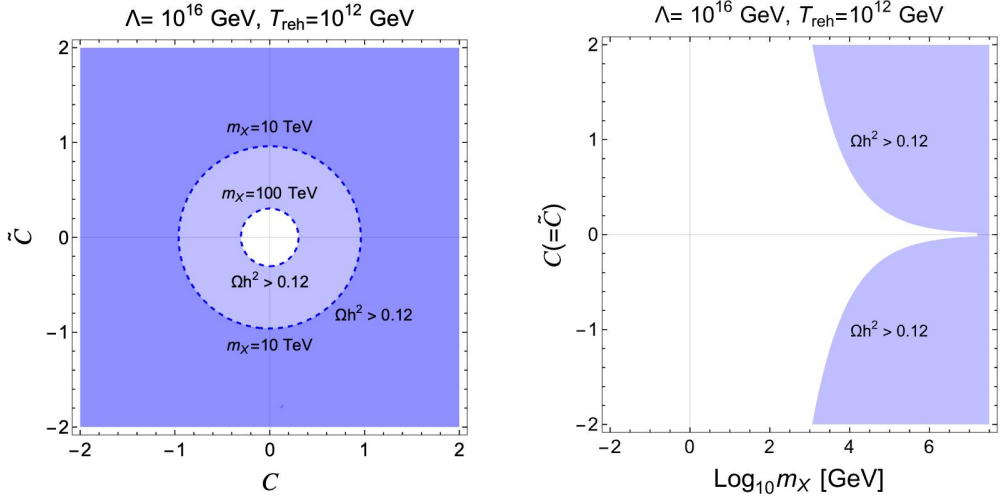


Figure 3: Left: Parameter space in the C - \tilde{C} plane. We take $m_X = 10$ TeV and 100 TeV. Right: Parameter space in the m_X - C ($= \tilde{C}$) plane. In all plots, we fix $\Lambda = 10^{16}$ GeV and $T_{\text{reh}} = 10^{12}$ GeV.

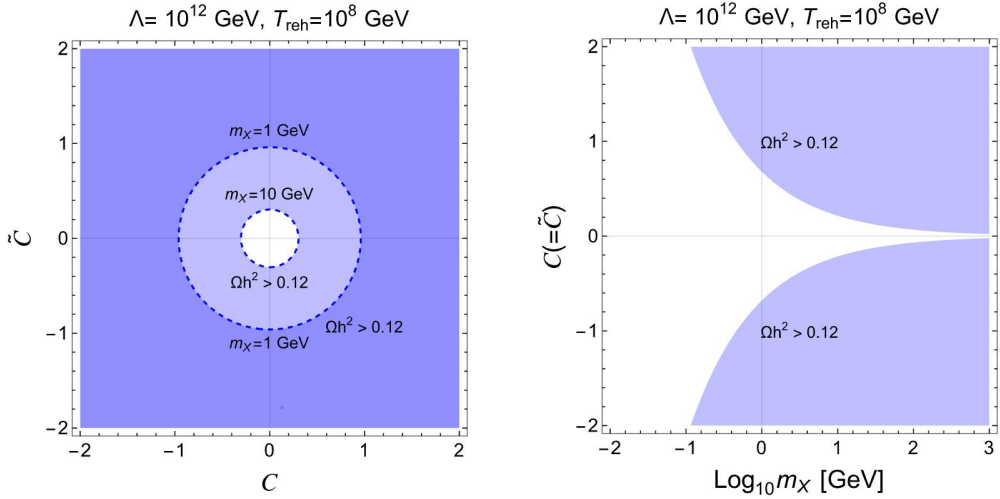


Figure 4: Same as Figure 3, but with $\Lambda = 10^{12}$ GeV and $T_{\text{reh}} = 10^8$ GeV. We choose $m_X = 1$ GeV and 10 GeV in the left panel.

3.3 Including Higgs-portal Operators from the Stueckelberg Mechanism

With the dimension-4 and dimension-6 Stueckelberg DM operators in addition to dimension-6 operators, we obtain the squared scattering amplitude for $\phi_i \phi_i \rightarrow XX$ ($i = 1, 2, 3, 4$) by

implementing the model in FeynRules [15–17] and using CalcHEP [18]:

$$\begin{aligned} |\mathcal{M}_{\phi_i\phi_i \rightarrow XX}|^2 &= \frac{2}{\Lambda^4} \left[C^2 (s^2 - 4m_X^2 s + 6m_X^4) + \tilde{C}^2 s (s - 4m_X^2) \right] \\ &\quad + \left(\lambda_{HX}^2 + \frac{s^2}{4\Lambda^4} C_X^2 - \lambda_{HX} C_X \frac{s}{\Lambda^2} \right) \left[\frac{s(s - 4m_X^2)}{4m_X^4} + 3 \right] \\ &\quad + \frac{3}{\Lambda^2} C \left(-2\lambda_{HX} + C_X \frac{s}{\Lambda^2} \right) (s - 2m_X^2), \end{aligned} \quad (53)$$

where the symmetry factors for identical particles in both the initial state ($\phi_i\phi_i$) and the final state (XX) are included. The spin states of the final-state DM (XX) are summed over. These Stueckelberg DM operators also give (s -wave)² contributions in Eq. (53). The energy growth of the amplitude from the dimension-4 Stueckelberg DM operator is consistent with Eq. (14). From Eq. (53), we observe an s^2 (or stronger) energy dependence, which is the same as that in Eq. (41) and implies UV freeze-in production.

In the high-energy limit, $s \gg m_X^2$, the squared scattering amplitude in Eq. (53) can be approximated as

$$|\mathcal{M}_{\phi_i\phi_i \rightarrow XX}|^2 \simeq \frac{2s^2}{\Lambda^4} \left(C^2 + \tilde{C}^2 \right) + \frac{s^2}{4\Lambda^4} \left(\bar{\lambda}_{HX} - \bar{C}_X \frac{s}{\Lambda^2} \right)^2, \quad (54)$$

where the barred parameters are related to the original ones as

$$\bar{\lambda}_{HX} = \lambda_{HX} \frac{\Lambda^2}{m_X^2}, \quad (55)$$

$$\bar{C}_X = C_X \frac{\Lambda^2}{2m_X^2}. \quad (56)$$

From Eqs. (21) and (22), these parameters satisfy

$$|\bar{\lambda}_{HX}| < 1, \quad |\bar{C}_X| < 1. \quad (57)$$

This follows from the fact that the effective scale required by perturbative unitarity must exceed the cutoff of the EFT.

In Eq. (54), we have ignored the mixing term of order $C\bar{C}_X s^2 m_X^2 / \Lambda^6$. This can be justified as follows. Taking the ratio of this term to the two terms of orders $C^2 s^2 / \Lambda^4$ (or $\tilde{C}^2 s^2 / \Lambda^4$) and $\bar{C}_X^2 s^4 / \Lambda^8$ in Eq. (54), respectively, we obtain

$$r_1 \simeq \frac{\bar{C}_X}{C} \frac{m_X^2}{\Lambda^2}, \quad r_2 \simeq \frac{C}{\bar{C}_X} \frac{\Lambda^2 m_X^2}{s^2} \simeq \frac{1}{r_1} \frac{m_X^4}{s^2}. \quad (58)$$

As long as $|r_1| \ll 1$ or $|r_2| \ll 1$, the mixing term can be neglected relative to either of the other two terms. This amounts to the following conditions:

$$\frac{\Lambda^2 m_X^2}{s^2} \ll \frac{|\bar{C}_X|}{|C|} \quad \text{or} \quad \frac{|\bar{C}_X|}{|C|} \ll \frac{\Lambda^2}{m_X^2}. \quad (59)$$

The EFT is valid in the regime characterized by $\Lambda^2 > \{s, m_X^2\}$. For our UV freeze-in case, we further have $s \gg m_X^2$. Taking $s = f\Lambda^2$ with $(0 <) f < 1$, the condition (59) reduces to

$$\frac{m_X^2}{\Lambda^2 f^2} \ll \frac{|\bar{C}_X|}{|C|} \quad \text{or} \quad \frac{|\bar{C}_X|}{|C|} \ll \frac{\Lambda^2}{m_X^2}. \quad (60)$$

If $|C| \geq |\bar{C}_X|$, the upper bound is automatically satisfied since $\Lambda^2 \gg m_X^2$. If $|C| < |\bar{C}_X|$, the lower bound is satisfied for $m_X^2/(\Lambda^2 f^2) \ll 1$. In the high-energy regime $s \gg m_X^2$ considered here, the definition of f implies $f \gg m_X^2/\Lambda^2$. Consequently, the lower bound becomes well below order unity. For instance, when $\Lambda = 10^{14}$ GeV and $m_X = 100$ GeV, we obtain $10^{-24} f^{-2} \ll |\bar{C}_X|/|C|$ or $|\bar{C}_X|/|C| \ll 10^{24}$. We also note that the mixing term vanishes in the limit $C \rightarrow 0$.

We find that the gauge-invariant dimension-6 operators dominate on DM production when the coefficients C and \tilde{C} are of order unity, since in Eq. (54), the squared amplitude becomes $|\mathcal{M}_{\phi_i \phi_i \rightarrow XX}|^2 \simeq 2(C^2 + \tilde{C}^2)s^2/\Lambda^4$. This is one conclusion for the DM production.

Next, we consider a different situation in which the coefficients C and \tilde{C} are smaller than order unity. Such a hierarchy of cutoff scales among the operators may arise if some operators are loop-suppressed, protected by symmetries, or associated with different UV cutoff scales. In this work, however, we do not specify the underlying UV theory and instead treat C and \tilde{C} as free parameters. Expanding Eq. (54) and ordering the terms by powers of s , we obtain

$$|\mathcal{M}_{\phi_i \phi_i \rightarrow XX}|^2 \simeq \frac{s^4}{4\Lambda^8} \bar{C}_X^2 - \frac{s^3}{2\Lambda^6} \bar{\lambda}_{HX} \bar{C}_X + \frac{s^2}{\Lambda^4} \left[2(C^2 + \tilde{C}^2) + \frac{1}{4} \bar{\lambda}_{HX}^2 \right]. \quad (61)$$

Compared to Appendix A of Ref. [9], the correspondences are

$$c_{4,0} = \frac{1}{4} \bar{C}_X^2, \quad c_{3,0} = -\frac{1}{2} \bar{\lambda}_{HX} \bar{C}_X, \quad c_{2,0} = 2(C^2 + \tilde{C}^2) + \frac{1}{4} \bar{\lambda}_{HX}^2, \quad M = \Lambda.$$

Therefore, in the limit of $T_{\text{reh}} \gg m_h$, the DM yield is given by

$$Y_X(m_h) \simeq 2 \times \frac{g_\phi}{\sqrt{g_*(T_{\text{reh}})}} (F_7 T_{\text{reh}}^7 + F_5 T_{\text{reh}}^5 + F_3 T_{\text{reh}}^3), \quad (62)$$

where

$$F_7 = \frac{32\sqrt{2/5} \pi^6 M_{\text{pl}} \bar{C}_X^2}{9261 \Lambda^8}, \quad (63)$$

$$F_5 = -\frac{108\sqrt{2/5} M_{\text{pl}} \zeta(5)^2 \bar{\lambda}_{HX} \bar{C}_X}{\pi^6 \Lambda^6}, \quad (64)$$

$$F_3 = \frac{\pi^2 M_{\text{pl}}}{540\sqrt{10} \Lambda^4} \left[2(C^2 + \tilde{C}^2) + \frac{1}{4} \bar{\lambda}_{HX}^2 \right]. \quad (65)$$

The DM relic density at present is determined as

$$\Omega_X h^2 = 1.6 \times 10^8 \left(\frac{m_X}{1 \text{ GeV}} \right) \left[\frac{g_{*s}(T_0)}{g_{*s}(T_{\text{reh}})} \right] Y_X(m_h). \quad (50)$$

As explained in Sec. 3.1, when the coefficients C and \tilde{C} are of order unity, the cutoff scale Λ typically needs to exceed the reheating temperature by about three orders of magnitude in order to satisfy the kinematic decoupling condition required for the freeze-in mechanism. If all coefficients are of similar order, the F_7 and F_5 terms can be safely neglected. However, since we treat the coefficients as more general free parameters, we keep these terms in the analyses. We consider two representative cases:

Case 1. All coefficients C , \tilde{C} , $\bar{\lambda}_{HX}$, and \bar{C}_X are of similar order. From Eq. (57), we focus on values of order 0.1.

Case 2. The coefficient \bar{C}_X is much larger than the others. Specifically, we take the coefficients to be $\bar{C}_X = 0.1 \gg \{C, \tilde{C}, \bar{\lambda}_{HX}\}$, with $C = \tilde{C}$.

In the following, we will discuss these two cases in turn.

Case 1. For Case 1, the F_7 and F_5 terms can be neglected. By replacing $C^2 + \tilde{C}^2$ with $C^2 + \tilde{C}^2 + \bar{\lambda}_{HX}^2/8$ in Eq. (52), the DM relic density is given by

$$\Omega_X h^2 \simeq 0.12 \left(\frac{m_X}{100 \text{ GeV}} \right) \left(\frac{T_{\text{reh}}}{10^{10} \text{ GeV}} \right)^3 \left(\frac{10^{14} \text{ GeV}}{\Lambda} \right)^4 \times 1.1 \left(C^2 + \tilde{C}^2 + \frac{1}{8} \bar{\lambda}_{HX}^2 \right). \quad (66)$$

For $C^2 + \tilde{C}^2 + \bar{\lambda}_{HX}^2/8 \simeq 0.01$, corresponding to Case 1, the DM mass required to reproduce the observed relic density is increased by approximately two orders of magnitude compared to the case in which only the gauge-invariant dimension-6 operators with $\mathcal{O}(1)$ coefficients are present. Alternatively, choosing a lower cutoff scale provides another viable option.

Note that the reheating temperature must be significantly lower than the cutoff scale (by roughly two or three orders of magnitude), to ensure the kinematical decoupling condition for the gauge-invariant dimension-6 interactions. Therefore, lowering the cutoff scale necessarily implies a corresponding reduction in the reheating temperature. However, since the relic density scales as Λ^{-4} , whereas it depends on the reheating temperature only as T_{reh}^3 , the relic density can still be enhanced by lowering the cutoff scale, even though the reheating temperature is simultaneously reduced.

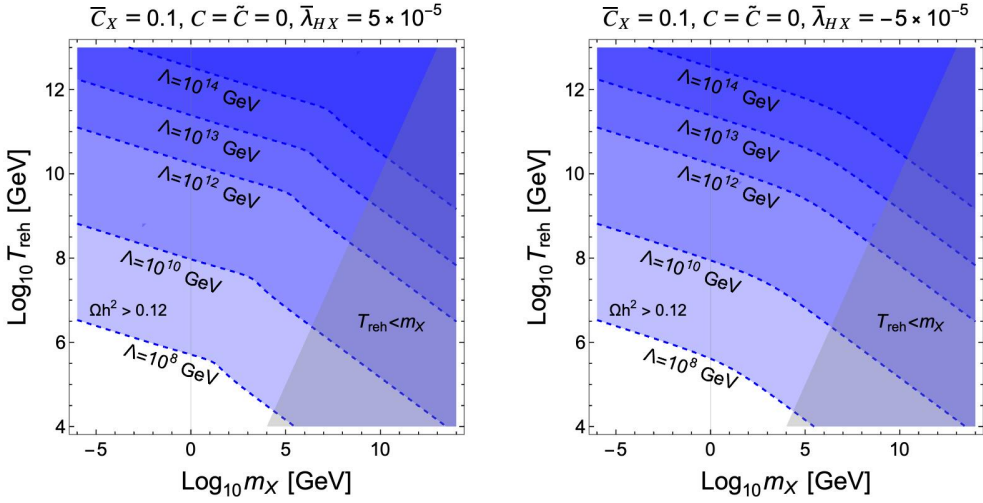


Figure 5: Same as Figure 2, but with a non-zero coupling $\bar{C}_X = 0.1$, whereas the gauge-invariant dimension-6 operators are set to zero, $C = \tilde{C} = 0$. In the left and right panels, we take $\bar{\lambda}_{HX} = 5 \times 10^{-5}$ and $\bar{\lambda}_{HX} = -5 \times 10^{-5}$, respectively. The cutoff scale is chosen as $\Lambda = 10^{8,10,12,13,14}$ GeV.

Case 2. For Case 2, in addition to the F_3 term, the F_7 and F_5 terms can also contribute to DM production. Since C and \tilde{C} enter the F_3 term in a similar manner, we take $C = \tilde{C}$. Although $\bar{\lambda}_{HX}$ also contributes in a similar way, it additionally enters the F_5 term through an interference effect with \bar{C}_X . Therefore, we do not assume $\bar{\lambda}_{HX}$ to have the same value as C and \tilde{C} .

In Figure 5, we show the parameter space in the m_X - T_{reh} plane that reproduces the observed DM relic density. For the cutoff scale, we take $\Lambda = 10^{8,10,12,13,14}$ GeV. We set the gauge-invariant dimension-6 operators to zero, $C = \tilde{C} = 0$, in order to see the effects of the F_5 term (arising from the interference between the Stueckelberg operators) and the F_7 term (from the dimension-6 Stueckelberg operator). We take $\bar{\lambda}_{HX} = 5 \times 10^{-5}$ in the left panel and $\bar{\lambda}_{HX} = -5 \times 10^{-5}$ in the right panel, respectively. Throughout this figure, we fix $\bar{C}_X = 0.1$. For a given cutoff scale, the F_7 term dominates at higher reheating temperatures, whereas the F_3 term becomes dominant at lower reheating temperatures in both panels. By comparing the left and right panels, one can also observe mild destructive (constructive) interference effects for positive (negative) values of $\bar{\lambda}_{HX}$. Note that, since the interference term F_5 in Eq. (64) is proportional to $\bar{\lambda}_{HX}\bar{C}_X$, the same effect can be obtained by flipping the sign of \bar{C}_X instead of $\bar{\lambda}_{HX}$.

In Figure 6, we present the parameter space in the $\bar{\lambda}_{HX}$ - C (= \tilde{C}) plane (left) and in the m_X - $\bar{\lambda}_{HX}$ plane (right) that reproduces the observed DM relic density. In the right panel, the gauge-invariant dimension-6 operators are set to zero, i.e., $C = \tilde{C} = 0$. Here, we fix

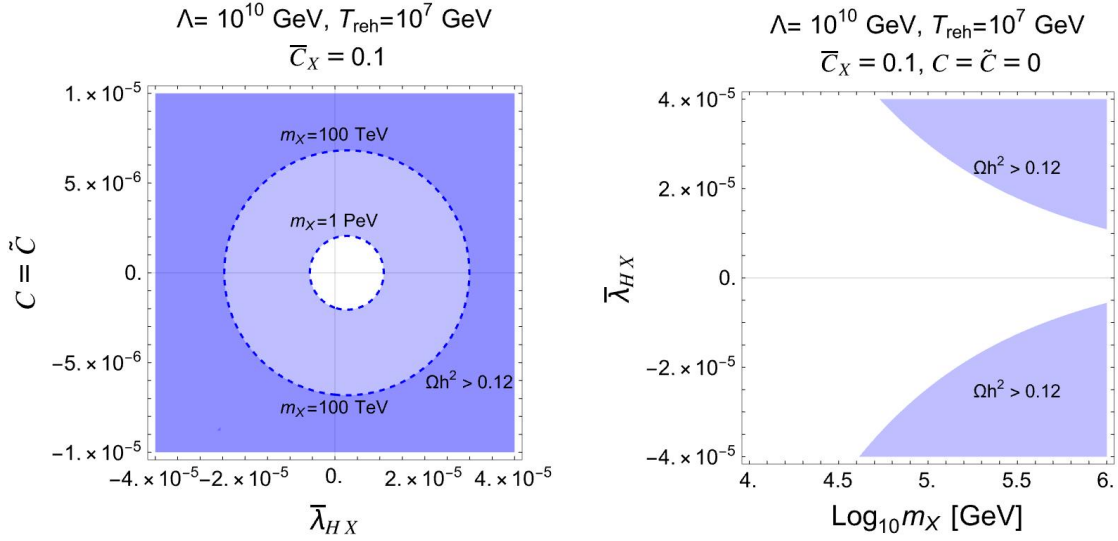


Figure 6: Left: Parameter space in the $\bar{\lambda}_{HX}$ - $C(= \tilde{C})$ plane. We take $m_X = 100$ TeV and 1 PeV. Right: Parameter space in the m_X - $\bar{\lambda}_{HX}$ plane. The gauge-invariant dimension-6 operators are set to zero, $C = \tilde{C} = 0$. In all plots, we fix $\bar{C}_X = 0.1$, $\Lambda = 10^{10}$ GeV, and $T_{\text{reh}} = 10^7$ GeV.

$\Lambda = 10^{10}$ GeV and $T_{\text{reh}} = 10^7$ GeV. In the left panel, for $m_X = 1$ PeV and $m_X = 100$ TeV, the boundaries corresponding to $\Omega_X h^2 = 0.12$ are obtained for small coefficients of order 10^{-6} - 10^{-5} . The boundary curves in the right panel indicate that $|\bar{\lambda}_{HX}|$ decreases as m_X increases. From both panels, we observe destructive (constructive) interference for positive (negative) values of $\bar{\lambda}_{HX}$.

Finally, we comment on the freeze-in DM production. One may wonder whether processes schematically of the form $XX \rightarrow \phi\phi$ (i.e., the inverse processes) could spoil DM production. The key point of the freeze-in mechanism is that the relevant reaction rates differ significantly between production and annihilation processes. The forward process, corresponding to the production of X from ϕ , has a reaction rate per unit volume given by $\Gamma_{\text{prod}} = n_\phi^2 \langle \sigma v \rangle$, where σ is the cross section and v is the relative velocity of the ϕ particles. If we suppose that, at the end of inflation, the Higgs field is produced much more abundantly than the X particles, then we would have $n_X \ll n_\phi$. Then, since the bath particles ϕ satisfy $n_\phi \simeq T^3$, for temperatures $T \geq m_X$, we obtain $\Gamma_{\text{prod}} \simeq T^6 \langle \sigma v \rangle$. In contrast, the DM annihilation rate is given by $\Gamma_{\text{ann}} = n_X^2 \langle \sigma v \rangle$. During freeze-in, however, the abundance of X is always much smaller than that of the thermal bath, $n_X \ll n_\phi \sim T^3$, and consequently $\Gamma_{\text{ann}} \ll \Gamma_{\text{prod}}$. We also assume that the ϕ fields do not reach thermal equilibrium, since $n_\phi \langle \sigma v \rangle < H$. This condition has been taken into account in Eqs. (28), (29), and (30). The particles X never reach thermal equilibrium either, because $n_X \langle \sigma v \rangle \ll n_\phi \langle \sigma v \rangle < H$. As a result, the

Boltzmann equation for the number density of X can be written as in Eq. (34).

4 Summary

We investigate a dark photon DM candidate X associated with a dark $U(1)_X$ gauge symmetry. In this setup, the assignment of a Z_2 -odd parity to X forbids kinetic mixing with the SM hypercharge. In this framework, the leading interactions arise from gauge-invariant dimension-6 Higgs-portal operators of both parity-even and parity-odd types. The dark photon mass is generated via the Stueckelberg mechanism, which additionally introduces a dimension-4 Higgs-portal interaction and further dimension-6 operators.

We focus on the freeze-in production of DM via Higgs-pair annihilation in the electroweak-symmetric phase after reheating, taking into account both the gauge-invariant dimension-6 operators and those induced by the Stueckelberg mechanism.

Using only the gauge-invariant dimension-6 operators, we identified viable regions of parameter space that reproduce the observed DM relic density for DM masses ranging from the keV scale up to tens of TeV, depending on the effective cutoff scale Λ and the reheating temperature T_{reh} . For example, a DM mass of $m_X \simeq 10$ TeV is compatible with $\Lambda \simeq 10^{16}$ GeV and $T_{\text{reh}} \simeq 10^{12}$ GeV, whereas the lightest allowed DM mass, $m_X \simeq \mathcal{O}(\text{keV})$, constrained by Lyman- α observations, can be realized for lower values of Λ and T_{reh} .

The Stueckelberg-induced contributions remain subdominant as a consequence of the requirement that the effective scale implied by perturbative unitarity be higher than the cutoff scale of the EFT. We found that when the coefficients of the gauge-invariant dimension-6 operators, C and \tilde{C} , are of $\mathcal{O}(1)$, these operators dominantly control the freeze-in production of DM.

We also explored a more general situation in which C and \tilde{C} are smaller than unity, as may occur if certain operators are loop-suppressed, protected by symmetries, or associated with different UV cutoff scales. In this case, all coefficients were treated as free parameters without specifying an explicit UV completion. In such scenarios, contributions with higher-order dependences on the reheating temperature, including interference effects, can become significant and lead to distinctive features in the DM parameter space.

We have thus extended previous studies by incorporating the freeze-in production scenario alongside the Stueckelberg mass generation mechanism in an EFT-consistent way. As an illustration of this more general regime, we find that the observed DM relic density can still be reproduced for parameter choices such as $m_X \simeq 100$ TeV, $\Lambda \simeq 10^{10}$ GeV, and $T_{\text{reh}} \simeq 10^7$ GeV, provided that one of the dimensionless coefficients is of 0.1, while the remaining three are of $\mathcal{O}(10^{-5})$. At the opposite end of the mass range, DM masses down to

$m_X \simeq \mathcal{O}(\text{keV})$, consistent with Lyman- α constraints, can again be realized for lower values of Λ and T_{reh} . This provides a promising mechanism for producing dark photons as feebly interacting massive particle DM across a wide range of masses and reheating temperatures.

Acknowledgements We have used the package TikZ-Feynman [21] to draw the Feynman diagrams. KY would like to thank Takashi Shimomura for valuable discussions. ST is supported by JSPS KAKENHI Grant No. 22K03642 and Waseda University Special Research Projects (Nos. 2025C-488 and 2025R-028). The work of KY was supported in part by JSPS KAKENHI Grant Number JP24K17040.

References

- [1] B. Holdom, Phys. Lett. B **166**, 196-198 (1986) doi:10.1016/0370-2693(86)91377-8
- [2] M. Fabbrichesi, E. Gabrielli and G. Lanfranchi, doi:10.1007/978-3-030-62519-1 [arXiv:2005.01515 [hep-ph]].
- [3] A. Caputo, A. J. Millar, C. A. J. O'Hare and E. Vitagliano, Phys. Rev. D **104**, no.9, 095029 (2021) doi:10.1103/PhysRevD.104.095029 [arXiv:2105.04565 [hep-ph]].
- [4] K. Yamashita, JHEP **10**, 205 (2024) doi:10.1007/JHEP10(2024)205 [arXiv:2407.01002 [hep-ph]].
- [5] G. D. Kribs, G. Lee and A. Martin, Phys. Rev. D **106**, no.5, 055020 (2022) doi:10.1103/PhysRevD.106.055020 [arXiv:2204.01755 [hep-ph]].
- [6] O. Lebedev, H. M. Lee and Y. Mambrini, Phys. Lett. B **707**, 570-576 (2012) doi:10.1016/j.physletb.2012.01.029 [arXiv:1111.4482 [hep-ph]].
- [7] H. Ruegg and M. Ruiz-Altaba, Int. J. Mod. Phys. A **19**, 3265-3348 (2004) doi:10.1142/S0217751X04019755 [arXiv:hep-th/0304245 [hep-th]].
- [8] E. Bertuzzo, T. Sassi and A. Tesi, JHEP **10**, 109 (2024) doi:10.1007/JHEP10(2024)109 [arXiv:2406.14437 [hep-ph]].
- [9] S. S. Kim, H. M. Lee and K. Yamashita, JHEP **11**, 119 (2023) doi:10.1007/JHEP11(2023)119 [arXiv:2308.14629 [hep-ph]].
- [10] Y. Mambrini, Particles in the dark Universe, Springer Cham (2021), doi:10.1007/978-3-030-78139-2
- [11] S. Dodelson and L. M. Widrow, Phys. Rev. Lett. **72**, 17-20 (1994) doi:10.1103/PhysRevLett.72.17 [arXiv:hep-ph/9303287 [hep-ph]].

- [12] L. J. Hall, K. Jedamzik, J. March-Russell and S. M. West, JHEP **03**, 080 (2010) doi:10.1007/JHEP03(2010)080 [arXiv:0911.1120 [hep-ph]].
- [13] N. Bernal, M. Heikinheimo, T. Tenkanen, K. Tuominen and V. Vaskonen, Int. J. Mod. Phys. A **32**, no.27, 1730023 (2017) doi:10.1142/S0217751X1730023X [arXiv:1706.07442 [hep-ph]].
- [14] N. Bernal, C. Cosme, T. Tenkanen and V. Vaskonen, Eur. Phys. J. C **79**, no.1, 30 (2019) doi:10.1140/epjc/s10052-019-6550-9 [arXiv:1806.11122 [hep-ph]].
- [15] N. D. Christensen and C. Duhr, Comput. Phys. Commun. **180**, 1614-1641 (2009) doi:10.1016/j.cpc.2009.02.018 [arXiv:0806.4194 [hep-ph]].
- [16] A. Alloul, N. D. Christensen, C. Degrande, C. Duhr and B. Fuks, Comput. Phys. Commun. **185**, 2250-2300 (2014) doi:10.1016/j.cpc.2014.04.012 [arXiv:1310.1921 [hep-ph]].
- [17] N. D. Christensen, P. de Aquino, C. Degrande, C. Duhr, B. Fuks, M. Herquet, F. Maltoni and S. Schumann, Eur. Phys. J. C **71**, 1541 (2011) doi:10.1140/epjc/s10052-011-1541-5 [arXiv:0906.2474 [hep-ph]].
- [18] A. Belyaev, N. D. Christensen and A. Pukhov, Comput. Phys. Commun. **184**, 1729-1769 (2013) doi:10.1016/j.cpc.2013.01.014 [arXiv:1207.6082 [hep-ph]].
- [19] Q. Decant, J. Heisig, D. C. Hooper and L. Lopez-Honorez, JCAP **03**, 041 (2022) doi:10.1088/1475-7516/2022/03/041 [arXiv:2111.09321 [astro-ph.CO]].
- [20] N. Aghanim *et al.* [Planck], Astron. Astrophys. **641**, A6 (2020) [erratum: Astron. Astrophys. **652**, C4 (2021)] doi:10.1051/0004-6361/201833910 [arXiv:1807.06209 [astro-ph.CO]].
- [21] J. Ellis, Comput. Phys. Commun. **210**, 103-123 (2017) doi:10.1016/j.cpc.2016.08.019 [arXiv:1601.05437 [hep-ph]].